D.B. (Don) Keele, Jr.
Audio Magazine
Hachette Magazines, Inc.
New York, NY 10019, USA

Presented at the 93rd Convention 1992 October 1–4 San Francisco

AN AUDIO ENGINEERING SOCIETY PREPRINT

The Analytic Impulse and the Energy-Time Curve: The Debate Continues

D. B. (Don) KEELE, JR.

Audio Magazine, Hachette Magazines, Inc., New York, NY 10019, USA
DBK Associates, Elkhart, IN 46517, USA

The analytic impulse is used as a complex-excitation signal to produce the Energy-Time Curve (ETC) of a system. The ETC, usually displayed on a wide-dynamic-range log scale, is the envelope of the system's impulse response and is loosely related to the energy decay in the system. Additional information is presented, using heuristic arguments and simulations, to show that: 1) The ETC is acausal in the same sense that the time response of a theoretical zero-phase filter is acausal; 2) A time-derivative-based complex-excitation signal (rather than a Hilbert-transform-based signal) does not work to extract the envelope of a system's impulse response; and 3) Even though the ETC is a good general approximation of the energy decay in a system, it does not predict details of the decay such as exact timing and rolloff behavior. The intent here is not to present any radical new information in this debate, but to explain and clarify some of the concepts.

0. INTRODUCTION

The energy-time curve (ETC), first presented by Heyser [1], [2] and used by others [3] - [5], is purported to show how the energy in a system decays as a function of time. The ETC and the related topic of the analytic impulse has been hotly debated [6], [7]. Even though the ETC has been closely associated with time-delay spectrometry [8], other implementation methodologies can be used to generate the ETC [9] - [12].

The primary inducement for the ETC is a need to display the impulse response of a system in a manner that allows easy identification of significant phenomena, both high and low level, and their times of occurrence. The ETC is usually plotted on a wide-dynamic-range logarithmic vertical axis versus time, so that low-level features can be seen as well as high-level features.

Duncan [6] points out that the ETC is inherently noncausal because the imaginary part of the analytic impulse excitation signal is derived using the Hilbert transform, which is itself noncausal because of very slow dropoff both before and after $t = 0$. In a real-world situation, however, measurements are always causal and appropriate steps are taken to minimise the noncausal behavior of the ETC such as windowing and appropriate delays.It works out that the ETC is most acausal for wide-bandwidth impulse responses. For narrow-band responses such as octave or one-third-octave reverberation decay measurements in auditoriums or concert halls, the noncausal nature of the ETC is minimal.

In this paper, I will show that the acausal nature of the ETC is closely akin to the acausalness of a zero-phase FIR filter. This type of filter needs to be delayed to make its response causal. Different processing and display methods for the impulse response will be illustrated, which leads to the need for the ETC. It will be shown that a time-derivative-based complex signal will not work for wide-band impulse response envelope extraction. Application of the ETC to a mechanical mass-spring-damper system will show that the ETC does not exactly predict energy decay, but does a good job in approximating the decay.

A mostly non-mathematical somewhat-tutorial treatment of these topics will be accomplished that depends heavily on simulation examples.

1. DISPLAY OF IMPULSE RESPONSE

The impulse response contains complete information about the workings of a linear time-invariant system. It is obtained by energizing the system with an impulse and then recording the output of the system as a function of time. The impulse response can be generated, as well, by alternate methods that do not actually apply an impulse to the system, such as swept sinewave [8] and pseudo-random noise [11]. In this section, I will display the impulse response of a simulated multiresonant system that both contains both high and low-level phenomena, with features that contain a wide range of frequencies. Different display methods will be illustrated leading to the ETC in the next section.

1.1. Simulated Multiresonant System

Fig. 1. shows the block diagram of a simulated multi-resonant system that also contains processing blocks that allow the impulse response to be measured and analyzed. The simulated multi-resonant system is composed of the parallel combination of three second-order bandpass filters with various parameters and delays. Parameters were chosen so that the impulse response frequency range covered an 8 to 1 ratio with various Q's, levels and delays, for each of the resonators. The following table lists the parameters of each of the band-pass filters:

TABLE 1: BAND-PASS FILTER CHARACTERISTICS

FILTER NUMBER	CENTER FREQUENCY Hz	Q	LEVEL dB	DELAY Secs
1	0.5	2	-10	5
2	2	2	0	0
3	4	4	-20	2.5

The levels were chosen so that the highest impulse response peak of each individual resonator has the indicated level. The Q of each resonator was chosen so that its impulse response decayed significantly before the next resonator was triggered.

All simulations were accomplished using the Apple Macintosh program "Extend" Vers. 1.1k (Highly recommended, an incredible program! Contact Bob Diamond at Imagine That, Inc., 151 Bernal Road, Suite 5, San Jose, CA 95119-1306, (408)-365-0305).

1.2. Scaling Of Linear Display

Fig. 2 shows various views of the impulse response of the simulated system of Fig. 1. All responses were plotted with a linear vertical amplitude scale over the range of 1 to 10 seconds. Three different expansion factors were selected, in decade ranges from 1 to 100, to show the both the high-level and low-level behavior of the response. With a linear vertical scale, it is not possible to see both high-level and low-level components of the impulse response on the same graph, thus the various expansion factors.

1.3. Log Display of Absolute Value

Fig. 3(a) shows the absolute value (full-wave rectified) of the impulse response plotted on a wide-dynamic-range 100 dB log scale. Note that as the signal passes through zero, the logged output of the absolute value actually goes to minus infinity. This generates a series of sharp vertical lines on the display at each point where the impulse response goes to zero. Because the simulation sample points do not coincide exactly with the zeros of the impulse response, the display does not go to large negative dB values at each zero point.

The display clearly shows the initial decay starting at 0 dB at 0 secs, followed by a higher-frequency decay starting at -20 dB at 2.5 secs, and a lower frequency decay commencing at 5 secs at a level of -10 dB. The sudden rises in level are clearly shown at the starting points of the three resonator responses at 0, 2.5 and 5 secs.

The rise and fall of the curve with each cycle of the impulse response is inherent to this type of display (logged absolute value). The curve clearly does not indicate the actual decay of energy in each resonator of the system, which should be a smoothly decreasing function. What is desired is the so-called envelope of the impulse response which should approximately follow the peaks of this display. Averaging the logged absolute value of the impulse response should yield a curve that comes close to this desired result.

1.4. Minimum-Phase First-Order Averaging

Figs. 3(b) and (c) show the effects of using a first-order minimum-phase low-pass filter to smooth the logged absolute value of the impulse response. Two different cutoff (-3 dB) frequencies were used in (b) and (c) to illustrate their effects.

In (b), a cutoff of 2 Hz was used to optimally smooth the 4-Hz highest frequency decay that commences at 2.5 secs. The lower frequency decays are seen to have much greater ripple in their response due to this high smoothing cutoff frequency. Some reduction in level of each peak is noted.

In (c), the cutoff frequency of the smoothing filter was lowered to 0.5 Hz to optimally smooth the lower frequency decay starting at 5 secs. Unfortunately, this low smoothing cutoff frequency severely distorts the shape of the two higher frequency decays between 0 and 5 secs.

1.5. Linear-Phase Averaging

Fig. 4 shows the effects of using a linear-phase 8th-order near-Gaussian smoothing filter (a 0.05° equiripple design was used that maintains constant delay out to the point at which the filter's response is 20 dB down). The constant delay of this type of filter shifts the output data to the right depending on the filters specific delay.

In (a), a filter cutoff frequency of 2.2 Hz was used, with a delay of 0.25 secs, to smooth the higher frequency decay. In (b), a lower filter cutoff of 0.55 Hz was used, with a delay of 1.00 secs, to smooth the lower frequency decay.

In (c), a superimposed plot of curve (b) with a one sec delayed version of the logged absolute value response of Fig. 3(a) is shown. This value of delay synchronizes the two curves. As can be seen, the linear-phase filtering does a much better job of approximating the envelope of the individual decays. Unfortunately, (c) shows appreciable noncausal-like behavior in the curve, because the response starts to rise significantly before the onset time of the individual resonators. This effect prevents the individual resonator decays from dropping down to their correct values at the time at which the next resonator comes in.

Note that smoothing, as was done in this and the previous section, cannot handle decay phenomena that cover a very wide frequency or time scale. The 8 to 1 range in input frequencies in Fig. 4 is just about the limit of envelope generation using smoothing of the logged absolute value of the impulse response. If the range were higher, say 100:1 or 1000:1, no single value of smoothing cutoff frequency would work for all the decays in the response. Of coarse, other schemes such as non-linear averaging, with different attack and decay times, have been tried.

2. THE ENERGY TIME CURVE

In order to get around the problems noted in the previous section, the energy time curve (ETC) was developed. This scheme depends on the use of a 90° phase shifter to generate an additional impulse-like response which is in phase quadrature to the original impulse response. This additional response (called the imaginary or quadrature response) is then combined with the original response (called the real or in-phase response) through a magnitude operation (square root of the sum of squares) to yield the envelope response. This scheme should theoretically work for all the frequencies in the impulse response, no matter how wide the range.

As Duncan points out [6, Section 1], the ETC can be computed in two different ways: 1. By measuring the conventional impulse response, calculating the quadrature response from the impulse response, and then combining the two, or 2. By separately measuring two responses, the impulse response (as before), and the response to a special impulse that is in phase quadrature to the original impulse, and then combining the two responses.

In the latter case (2.), the real question is what is the form of the special impulse that is in phase quadrature to the regular impulse? The regular impulse is, of coarse, the familiar Dirac delta function $\delta(t)$, using the symbols and nomenclature of [6].

The next two sections consider the two main contenders for the definition of the impulse that is in phase quadrature to the regular impulse: the Hilbert-transform-based definition, and the time-derivative-based definition. Both definitions yield an impulse whose frequency components are all 90° out-of-phase with the corresponding frequency components of the regular impulse. But as will be shown, only one of the two yield a frequency spectrum for the quadrature-phase impulse that is flat and equal to the spectrum of the regular impulse. This will be shown to be very crucial for proper envelope calculation.

2.1. Hilbert-Transform-Based Analytic-Impulse Excitation

If the Hilbert transform [7, eq. (4)] is used to calculate the quadrature-phase impulse from the regular impulse, the complete analytic-impulse signal is formed. Using complex terminology, the analytic impulse $\nabla(t)$ is a complex signal with real part equal to the delta function $\delta(t)$, and imaginary part equal to the Hilbert transform of the delta function $(1/(\pi t))$. These two signals are shown in Fig. 5(a). As can be seen, the imaginary part of the analytic impulse decays very slowly on either side of t = 0.

To calculate the ETC of a system (using the second method), the individual responses to the real and imaginary parts of the analytic signal must be measured. These two responses are then combined in a magnitude operation (square root of the sum of squares) to yield the ETC.

The individual responses of the system in Fig. 1, to the real and imaginary parts of the analytic impulse, are shown in Fig. 5(b) and (c), plotted over the range of -1 to 10 secs with linear vertical scale. The simulation was run over a range of -20 to +20 secs with 5000 steps, using double-precision floating-point calculations (this took about 90 secs on a Mac SE/30).

Fig. 6 shows the resultant ETCs plotted on a 100 dB log scale. Fig. 6(a) shows the data plotted over the range of -10 to +10 secs. This essentially eliminated from the graph the startup transients due to starting the simulation at -20 secs (the simulation should be started at time minus infinity theoretically!). Fig. 6(b) shows the data over 0 to +10 secs and should be compared to the previous graphs. (c) shows the ETC superimposed with the logged absolute data of Fig. 3(a).

As can be seen from (c), the ETC does a good job of deriving the envelope for all three of the decays. Note that no averaging was done here. The peak levels and timings of the start of the decays were also preserved well. Unfortunately, the acausal nature of the ETC significantly modifies the decays near their lower levels, at points just preceding the next decay peak.Steps can be taken to minimize the acausal effects of the ETC by windowing is spectrum in the frequency domain. The beneficial effects of using a cosine squared window are illustrated well in [6].

Comparing Figs. 4(c) and 6(c) show that the acausal nature of the ETC is quite comparable to the equivalent acausal nature of the linear-phase filter used to smooth the rectified impulse data.

Windowing in the frequency domain regrettable, directly modifies the frequency content of the ETC and may cause false estimates of the relative levels of different frequency ranges of a specific response [7, Section 2.].

2.2. Time-Derivative-Based Complex Excitation

If the time-derivative operation is used to calculate the quadrature-phase impulse from the regular impulse [1], [6, Appendix I], an alternate complex signal is formed which is causal. With this signal, the real and imaginary parts are indeed in phase quadrature. However, the spectral content of the real and imaginary parts are not equal.

Fig. 7 displays the spectrum magnitude of the real and imaginary parts of both the analytic impulse and the complex signal based on the derivative operation. Although the spectrum magnitudes of the real parts of both signals are flat (independent of frequency), only the imaginary part of the analytic impulse is flat and identically equal to the real part.

The spectral magnitude of the imaginary part of the derivative-based signal starts at zero at zero frequency, and then rises indirect proportion to frequency. The spectral magnitude of the imaginary part of the derivative-based signal is only equal to the real part at one frequency f_E. Adjusting the level of the imaginary part of the signal in relation to the level of the real part, serves to position f_E at any arbitrary frequency. This is equivalent to rotating the imaginary magnitude line around the origin. As will be illustrated, only at and near f_E will this test signal properly yield the envelope of the impulse response.

Fig. 8 shows the envelopes measured using the derivative-based complex signal plotted on a 100 dB log scale. The level of the imaginary part of the signal was adjusted to optimally construct the envelope for different frequency decays. The level was adjusted in (a) and (b) to yield the correct envelope for the highest frequency decay between 2.5 and 5 secs of the response. In (c), the level was adjusted to properly yield the envelope for the lowest frequency decay, which starts at 5 secs. In both cases, the envelope is calculated properly only for one of the decays. Note the higher level of (c) relative to (b) as a result of the raised imaginary part. Note that all the derivative-based envelope plots do not exhibit any acausal effects.

3. DOES THE ETC EXACTLY PREDICT DECAY ENERGY DECAY IN A SYSTEM?

Heyser implied that the ETC corresponds to the energy flow or decay in a system [1, Appendix Part III]. Here I investigate this claim by computing the true energy decay in a simulated second-order mechanical system and then compare this result with the ETC of the same system.

3.1. Simulated Mass-Spring-Damper System

Fig. 9 shows the block diagram of a simulated second-order mass-spring-damper system. An unconstrained mass was attached to an unmovable object with a parallel combination of spring and damper. The motion of the mass was simulated after applying an impulse of force (like a hammer blow) to the mass. The resultant displacement and velocity were used to calculate the total energy decay. The parameters of the simulated system were: mass = 1 kg, spring constant = 1 N/m, and damping coefficient = 0.1 N/m/s. The simulation was run with 4,000 steps over 0 to 160 secs with the impulse of force applied at t = 80 secs.

3.2. True Energy Decay

The energy decay in the mass-spring-damper system of Fig. 9 was calculated by computing the individual potential ($1/2 \cdot kx^2$) and kinetic energies ($1/2 \cdot mv^2$), where k = spring constant, x = displacement, m= mass, and v = velocity, then summing to yield the true total energy decay of the system.

Fig. 10(a) shows the predicted displacement (dark curve) and velocity (light curve) of the mass. Fig. 11 shows the resultant total energy of the system plotted against time in three different ways. Fig. 11(a) shows a superimposed plot of the total energy (dark curve) with the potential (medium curve) and kinetic (light curve) energies plotted on a linear vertical scale. Fig. 11(b) is a plot of total energy plotted on a linear vertical scale. Fig. 11(c) is a plot of total energy plotted on a 60 dB log vertical scale over a wider time span of 70 to 140 secs. (c) shows a sudden jump in total system energy at t = 80 secs, and then a smooth linear decrease of energy (logged) over the remaining simulation time.

Note that the energy does not decay in a purely exponential manner, but in a sequence of small smoothed steps synchronized with the oscillation. This completely baffled me originally because I was expecting a purely exponential decay curve for the total energy ie $E(t) = E_1 e^{-t/\tau}$. Further thought revealed that the energy loss is not continuous but is only lost in the damper when the mass is in motion. Maximum energy loss occurs at points of maximum velocity (zero displacement), and energy loss is zero when the mass is rest (points of maximum displacement and zero velocity).

3.3. ETC-Predicted Energy Decay

In parallel display with Fig. 11, Fig. 12 shows various plots of the ETC of the mass-spring-damper system. The ETC was generated by applying an impulse to yield the displacement function, which is the real part of the ETC, and then calculating the response to Hilbert transformed impulse (Fig. 5(a) light curve), which is the imaginary part of the ETC. As before the simulation extended over 0 to 160 secs with the analytic impulse applied at t = 80 secs.

Fig. 12(a) shows a superimposed plot of the magnitude of the ETC (dark curve), the real part of the ETC (light curve, corresponds to previous potential energy), and the imaginary part of the ETC (medium curve, corresponds to previous kinetic energy), all plotted on a linear vertical scale. Fig. 12(b), plot of ETC on linear vertical scale. Fig. 12(c), plot of ETC on a 60 dB log vertical scale over a wider time scale of 70 to 140 secs.

Compare the plots in this figure with the true energy decay in Fig. 11. Note the rounding of the initial peak and the acausal build up of energy before the impulse which is a characteristic of the ETC. Note also that the small variations in the decay do not agree with the true energy decay of Fig. 11, ie, the cyclic loss of energy exhibited by the true energy decay is not shown in the ETC. All things considered, the ETC of Fig. 12(c) is a good approximation of the true energy decay in Fig. 11c.

4. CONCLUSIONS

I have shown through simulation examples several means for displaying the envelope of the impulse response of a system. These included: 1. scaled plots of the impulse response plotted on a linear vertical scale, 2. plots of the absolute value of the impulse response plotted on a log vertical scale, 3. plots of the averaged (using both minimum-phase and linear-phase filtering) absolute value of the impulse response plotted on a log vertical scale, and 4. ETC plots.

It was shown that linear-phase smoothed absolute value of the impulse response did a reasonably good job of extracting the envelope, but operated only over a limited range of about 8 to 1 in impulse spectral frequency range. The linear-phase smoothing exhibited significant acausal effects.

The ETC did the best job of extracting the envelope for wide frequency range signals but also suffers from significant acausal effects. It was shown that the acausal effects of the ETC are similar to the acausal effects of using a linear-phase filter to smooth the full-wave rectified impulse response.

The time-derivative-based envelope technique was shown to operate well only over a narrow frequency range. However, this technique did not exhibit any acausal effects, which might make it very useful for some situations.

A mass-spring-damper system was analyzed to show that the ETC is a good approximation of the true energy decay in the system.

5. REFERENCES

[1] R. C. Heyser, "Determination of Loudspeaker Signal Arrival Times, Parts I, II, and III," *J. Audio Eng. Soc.*, vol. 19, pp. 734-743 (1971 Oct.); pp. 829-834 (1971 Nov.); pp. 902-905 (1971 Dec.).

[2] R. C. Heyser and D. H. Le Croissette, "A New Ultrasonic Imaging System Using Time Delay Spectrometry," *Ultrasound Med. Biol.*, pp. 119-131 (1974).

[3] P. M. Gammell, "Improved Ultrasonic Detection Using the Analytic Signal Magnitude," *Ultrasonics*, vol. 19, pp. 73-76 (1981 Mar.).

[4] P. M. Gammell, "Analogue Implementation of Analytic Signal Processing for Pulse-Echo Systems," *Ultrasonics*, vol. 19, pp. 279-283 (1981 Nov.).

[5] P. D'Antonio and J. Konnert, "Complex Time-Response Measurements Using Time-Delay Spectrometry," *J. Audio Eng. Soc.*, vol. 37, pp. 674-690 (1989 Sept.).

[6] A. Duncan, "The Analytic Impulse," *J. Audio Eng. Soc.*, vol. 36, pp. 315-327 (1988 May).

[7] J. Vanderkooy and S. P. Lipshitz, "Uses and Abuses of the Energy-Time Curve," *J. Audio Eng. Soc.*, vol. 38, pp. 819-836 (1990 Nov.).

[8] R. C. Heyser, "Acoustical Measurements by Time Delay Spectrometry," *J. Audio Eng. Soc.*, vol. 15, pp. 370-382 (1967 Oct.).

[9] P. M. Gammell, "Coherent Processing of the Full Analytic Signal Information of Ultrasonic Waveforms," International Advances in Non-destructive Testing, vol. 10, Gorden and Breech Publishers (1984).

[10] S. P. Lipshitz, T. C. Scott, and J. Vanderkooy, "Increasing the Audio Measurement Capability of FFT Analyzers by Microcomputer Postprocessing," *J. Audio Eng. Soc.*, vol. 33, pp. 626-648 (1985 Sept.).

[11] D. D. Rife and J. Vanderkooy, "Transfer Function Measurement with Maximal Length Sequences," *J. Audio Eng. Soc.*, vol. 37, pp. 419-444 (1989 June).

[12] R. Greiner, J. Wania, and G. Noejovich, "A Digital Approach to Time-Delay Spectrometry," *J. Audio Eng. Soc.*, vol. 37, pp. 593-602 (1989 July/Aug.).

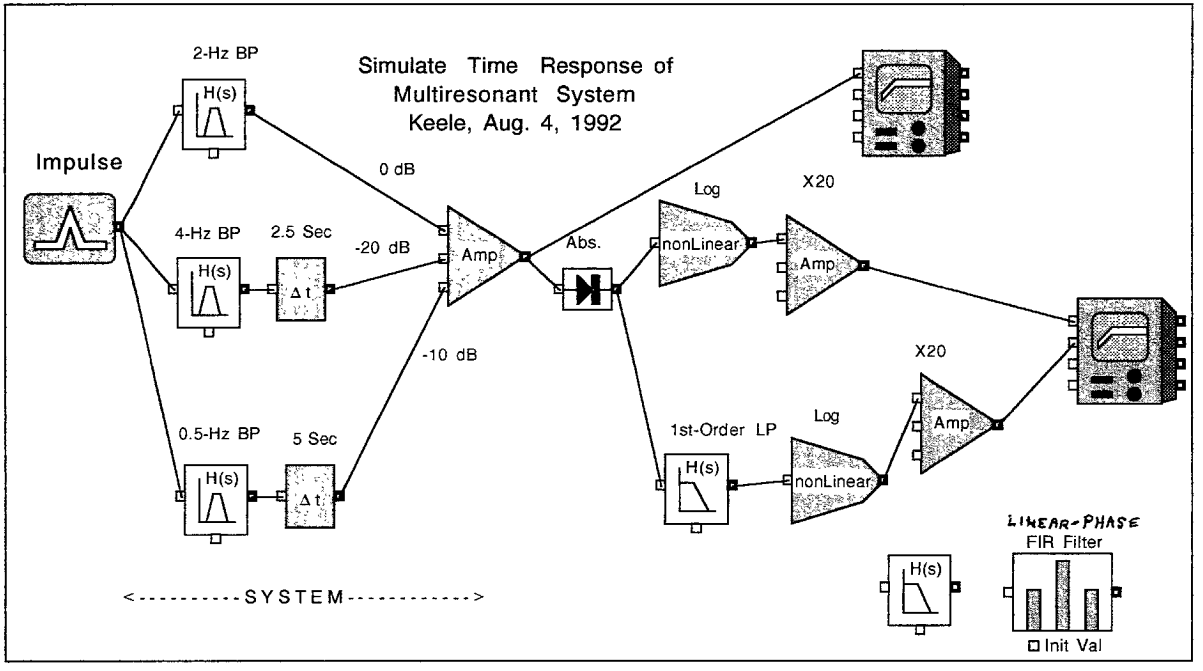

Fig. 1. Block diagram of a simulated multi-resonant system used to model different forms of impulse response analysis methods. The system is composed of the summed output of three second-order bandpass filters with various parameters: 1. an undelayed 2-Hz filter with unity impulse output, 2. a 4-Hz filter delayed 2.5 secs with output attenuated 20 dB, 3. a 0.5-Hz filter delayed 5 secs with output 10 dB down. Additional blocks are included to energize the system and analyze/plot its output.

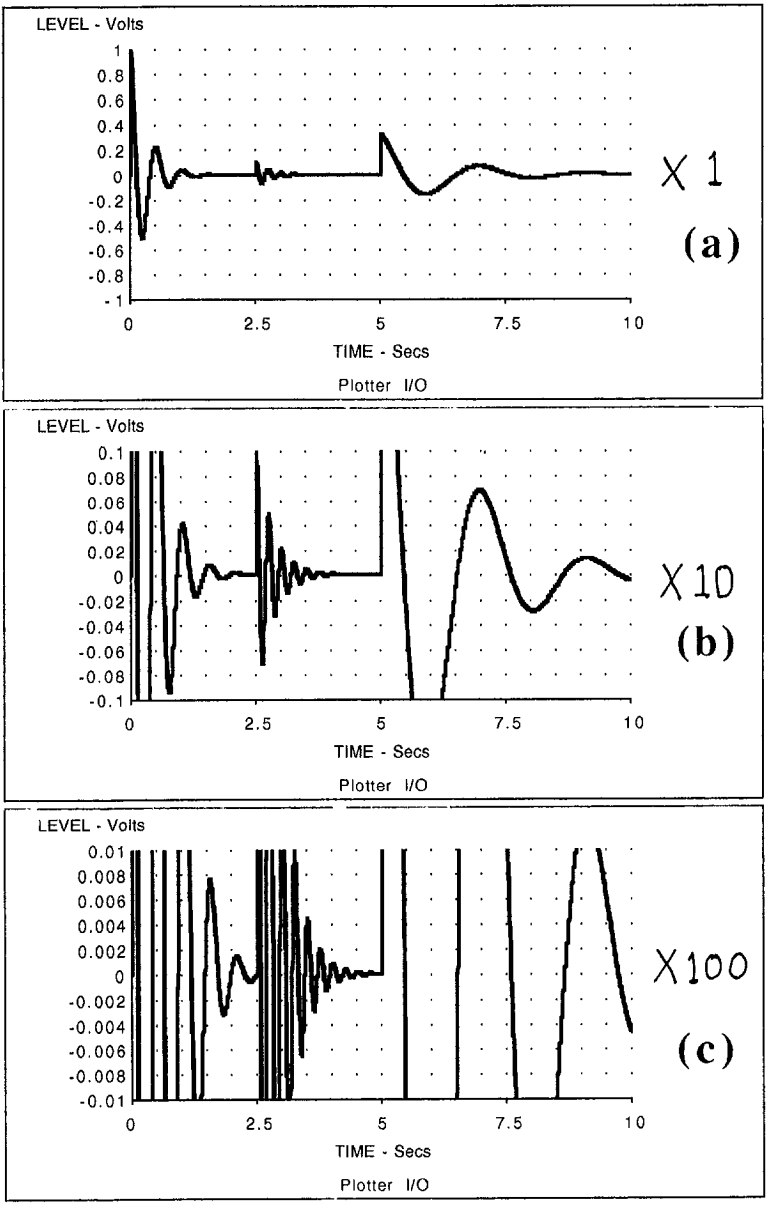

Fig. 2. Impulse response of the system modeled in Fig. 1, plotted on a linear amplitude scale at various amplifications. (a) Times one amplification. (b) Times ten amplification. (c) Times one-hundred amplification.

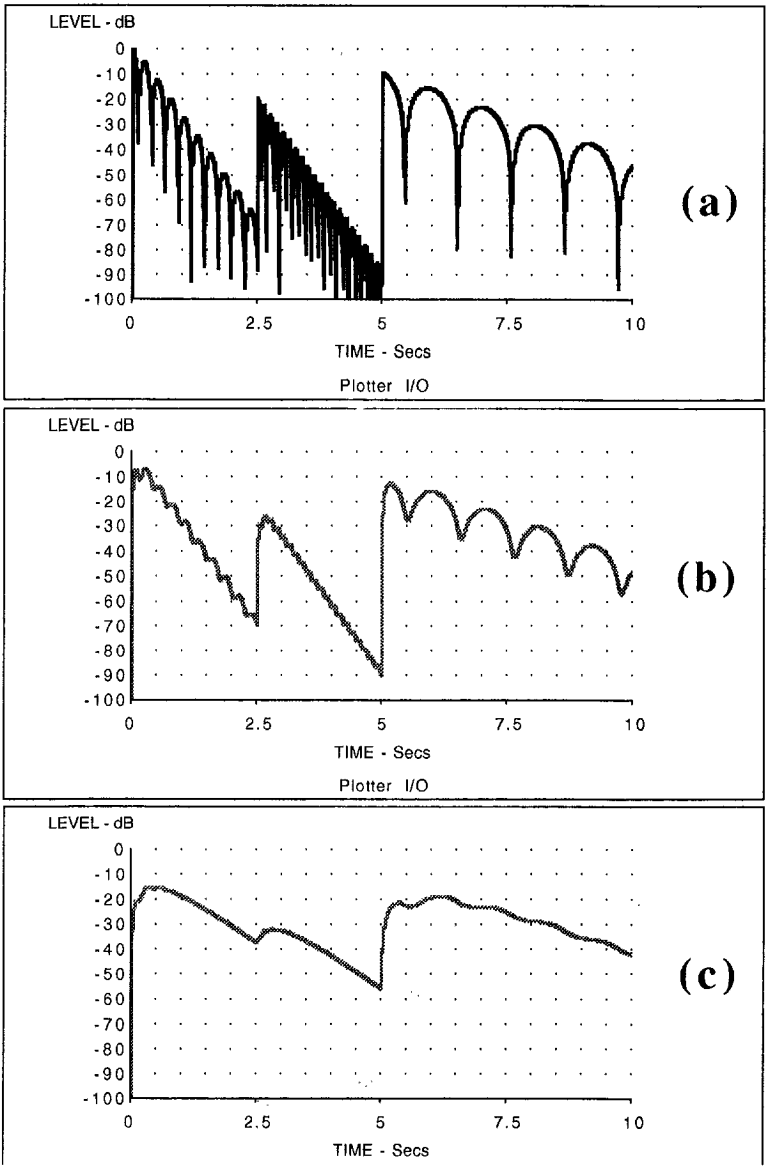

Fig. 3. Impulse response of the system modeled in Fig. 1, plotted in various ways. (a) Absolute value of impulse response plotted on a 100 dB log scale. (b) Absolute value of impulse response smoothed with a first-order 2-Hz (-3 dB) minimum-phase low-pass filter. (c) Absolute value of impulse response smoothed with a first-order 0.5-Hz low-pass filter. The smoothing in (b) works well for the high-frequency decay, but not well for the lower-frequency responses. The smoothing in (c) works well for the low-frequency decay, but swamps the decay of the higher-frequency responses.

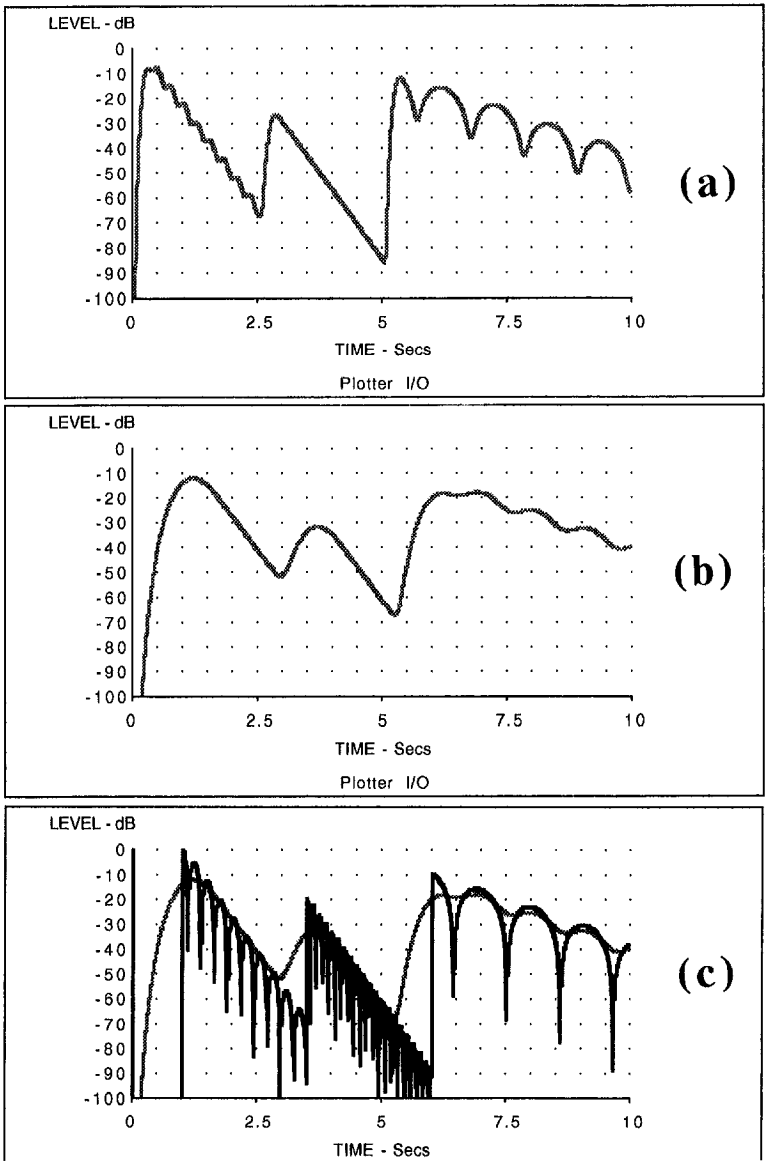

Fig. 4. Linear-phase smoothed impulse responses of the system modeled in Fig. 1. (a) Absolute value of impulse response smoothed with a 2.2-Hz Gaussian low-pass filter with a delay of 0.25 sec. (b) Absolute value of impulse response smoothed with a 0.55-Hz Gaussian low-pass filter with a delay of 1.00 sec. (c) Superimposed plot of the smoothed data of (b) with the unsmoothed data of Fig. 3 (a) delayed by one second. The linear-phase filtering works significantly better than the first-order filtering of Fig. 3 in yielding the shape of the impulse decay. As before however, a lower cutoff frequency works well for the low-frequency responses, but not for the high-frequency responses, and vice-versa.

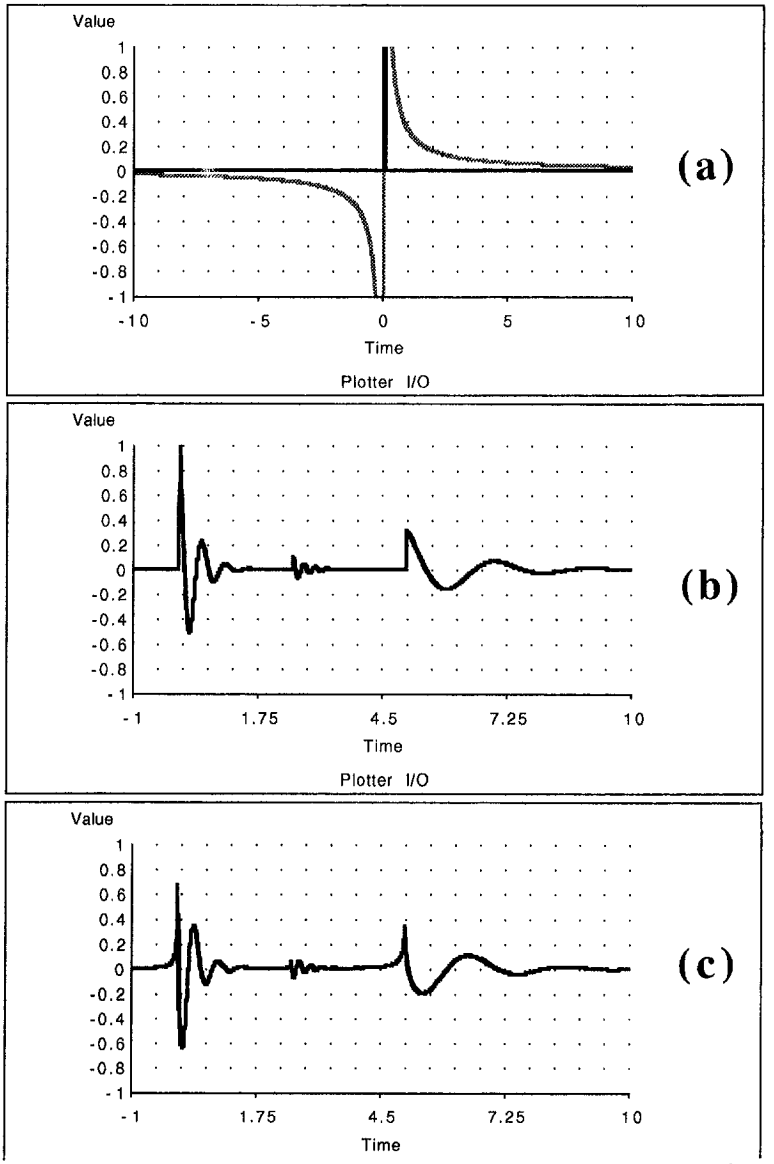

Fig. 5. Plot of the real and imaginary parts of the analytic impulse, and the responses of the system modeled in Fig. 1 to the individual parts of the analytic impulse. (a) The real part (dark line) and imaginary part (light line) of the analytic impulse excitation signal. (b) Response of the system to the real part of the analytic impulse plotted on a linear vertical scale over the range of -1 to 10 secs. (c) Response of the system to the imaginary part of the analytic impulse plotted on a linear vertical scale over the range of -1 to 10 secs. The magnitude of (b) and (c), considered jointly, constitute the ETC.

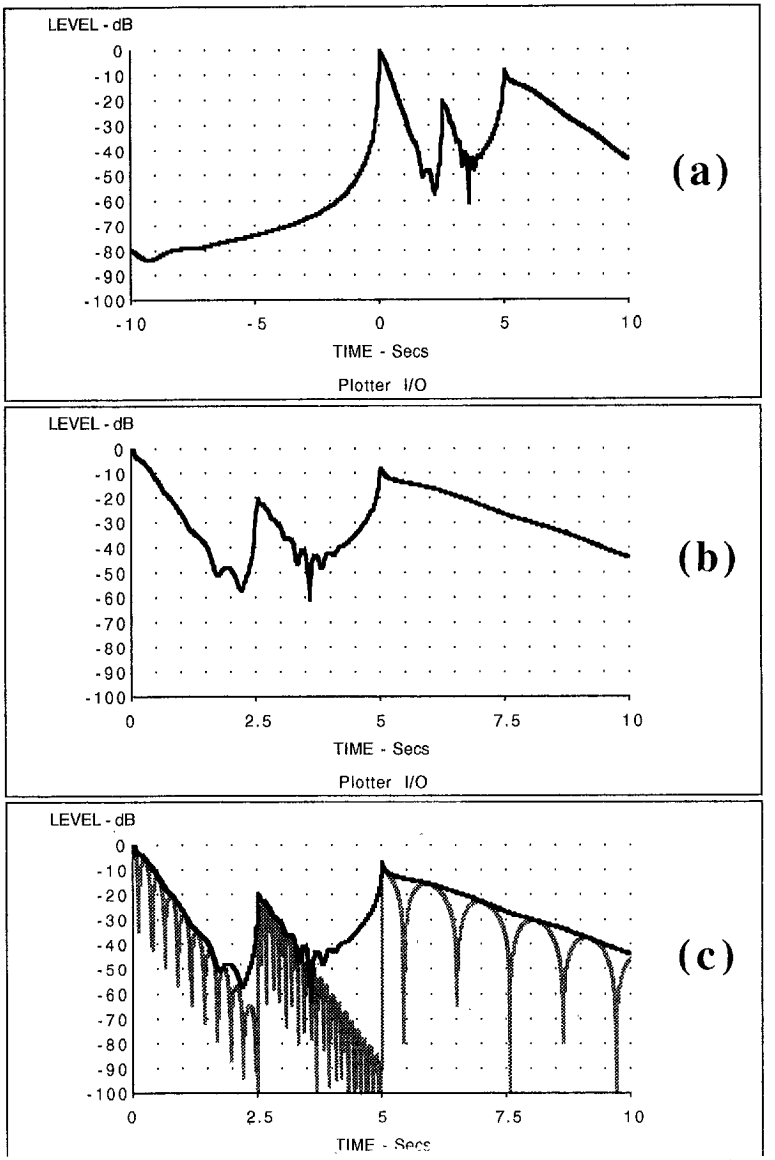

Fig. 6. ETC magnitude plots of the analytic impulse response of the system modeled in Fig. 1 [responses of Fig. 5 (b) and (c)], plotted on a 100 dB log scale. (a) ETC plotted over the range of -10 to 10 secs. (b) ETC plotted over the range of 0 to 10 secs. (c) Superimposed plot of the ETC data of (b) with the unsmoothed data of Fig. 3 (a). Note that the ETC closely follows the decay of each individual response, but suffers from significant acausal-like anticipatory effects that precede each decay peak.

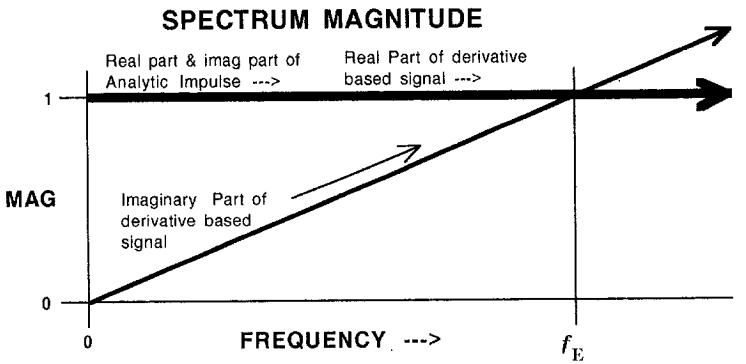

Fig. 7. Display of the spectrum magnitudes of the individual real and imaginary parts of the analytic impulse excitation signal, and the time-derivative-based complex excitation signal, plotted for positive frequencies. Note that the magnitudes of the real and imaginary parts of the analytic signal are equal and independent of frequency. Note also that the magnitudes of the real and imaginary parts of the time-derivative-based complex signal are only equal at one frequency (f_E). The imaginary part starts out at zero and rises directly proportional to frequency. The level of the imaginary part of the time-derivative-based complex signal can be adjusted to position f_E at any frequency (equivalent to rotating the imaginary magnitude line around the origin). Only at and near f_E does this signal properly form the envelope of the impulse response.

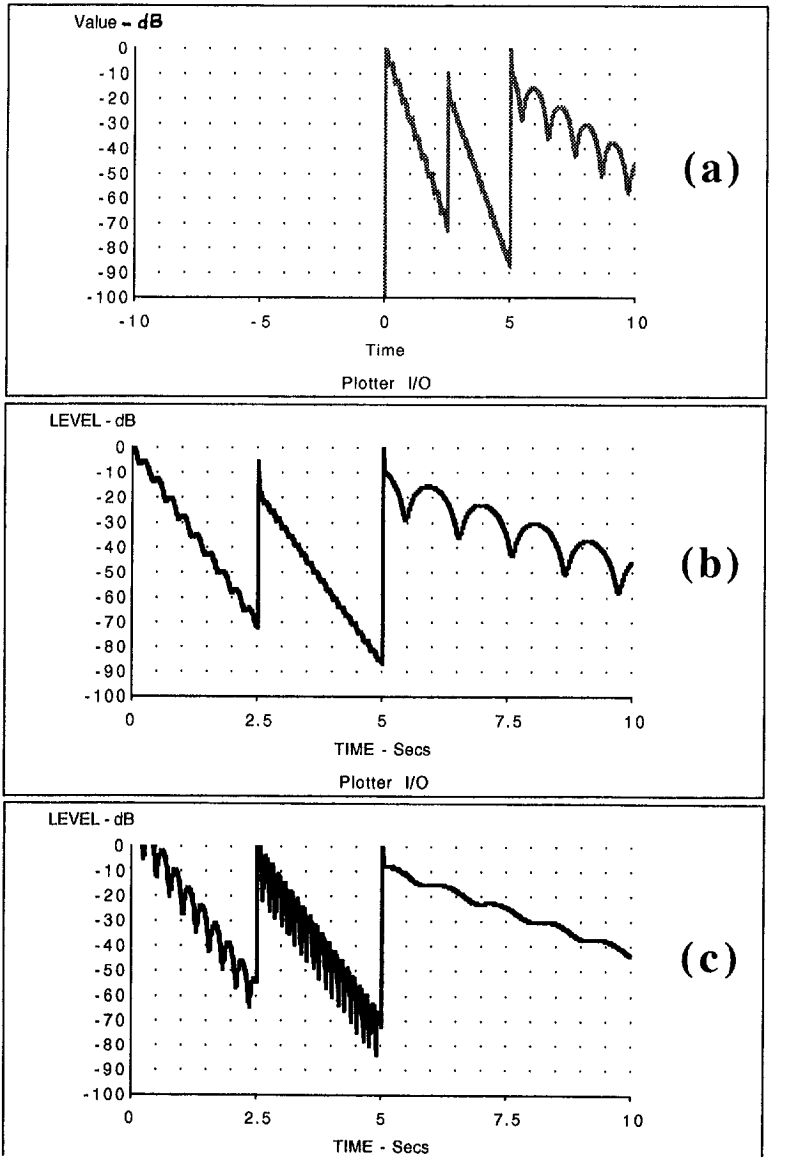

Fig. 8. Envelope magnitude plots of the response of the system modeled in Fig. 1 to the time-derivative-based complex signal, plotted on a 100 dB log scale. The envelope is calculated by combining the impulse response and a scaled doublet response. (a) Envelope response plotted over the range of -10 to +10 secs. The level of the imaginary part of the test signal was adjusted to properly extract the envelope of the highest frequency part (middle decay) of the system's response. Note the absolutely causal behavior of the response, ie no false envelope is seen to exist before the onset of the decays. (b) Envelope response of (a) but plotted over the range of 0 to +10 secs. Compare (b) to the ETC of Fig. 6 (b). (c) Envelope response plotted over the range of -10 to +10 secs. The level of the imaginary part of the test signal was raised to properly extract the envelope of the lowest frequency part (third decay) of the system's response. Note the higher level of (c) relative to (b) as a result of the raised imaginary part. Note also that for a specific imaginary-part level, the envelope extraction only works well for a narrow frequency range.

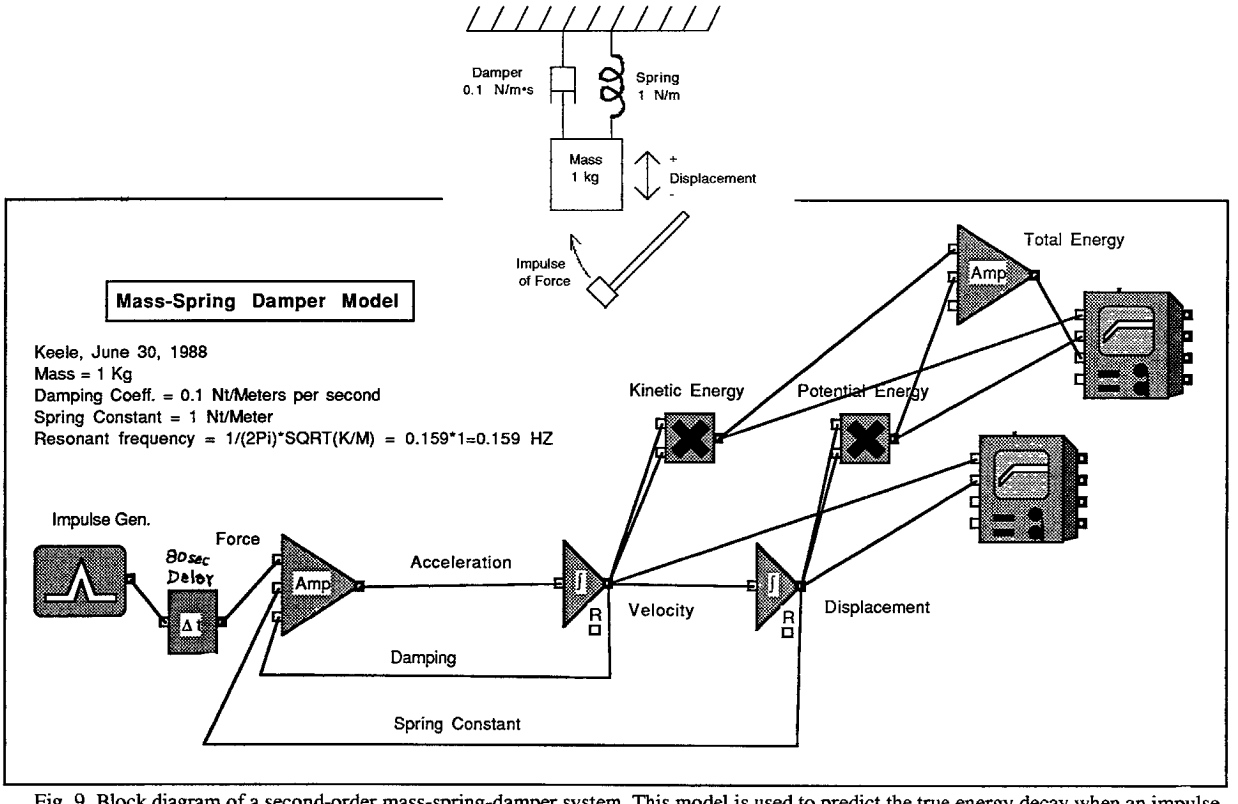

Fig. 9. Block diagram of a second-order mass-spring-damper system. This model is used to predict the true energy decay when an impulse of force is applied to the mass. The system is originally at rest. A standard analog computer configuration, using feedback around two integrators, predicts the displacement and velocity of the mass after a force is suddenly applied. The potential and kinetic energies are then summed to yield the total energy decay of the system. Alternately, the ETC is calculated by separately applying the real and imaginary parts of the analytic impulse and then plotting the square root of the sum of squares of the resultant displacement. The following physical parameters were used in the simulation: mass = 1 kg, spring constant = 1 N/m, and damping coefficient = 0.1 N/m/s. This results in a resonant frequency of 0.159 Hz with moderate damping. A 4,000 step simulation was accomplished over the range of 0 to 160 secs. A block was inserted to delay the applied impulse by 80 secs.

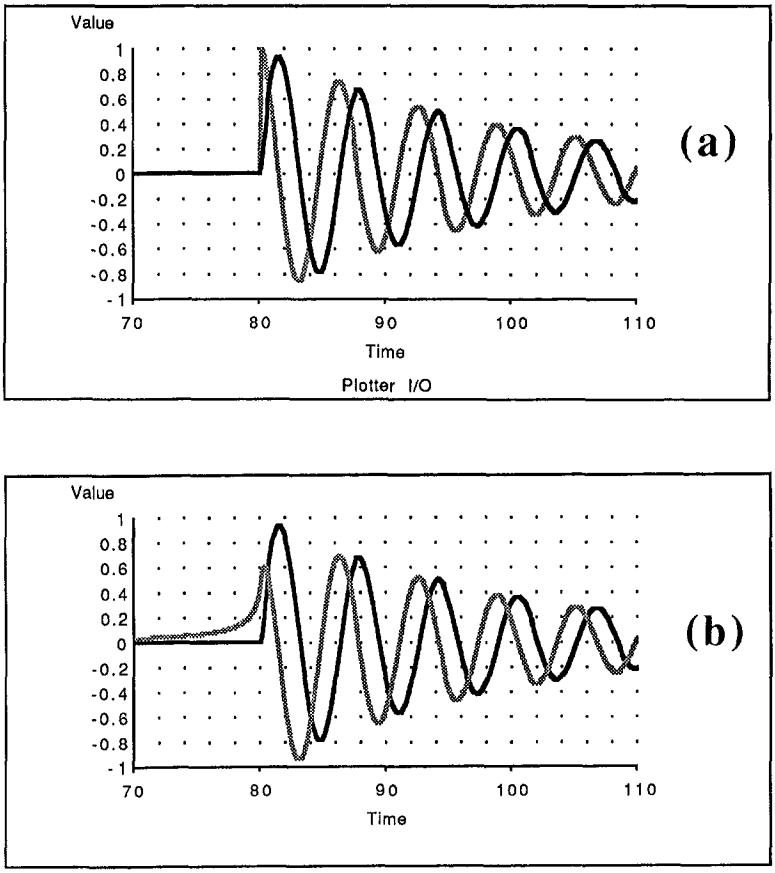

Fig. 10. Plots of the scaled velocity and displacement for the mass-spring-damper system of Fig. 9. (a) Displacement (dark curve) and velocity (light curve) of mass. (b) Displacement (dark curve) and Hilbert transform of displacement (light curve). In (b), the real and imaginary parts of the analytic signal were applied separately to yield the resultant curves. Correct relative amplitudes are preserved in these plots.

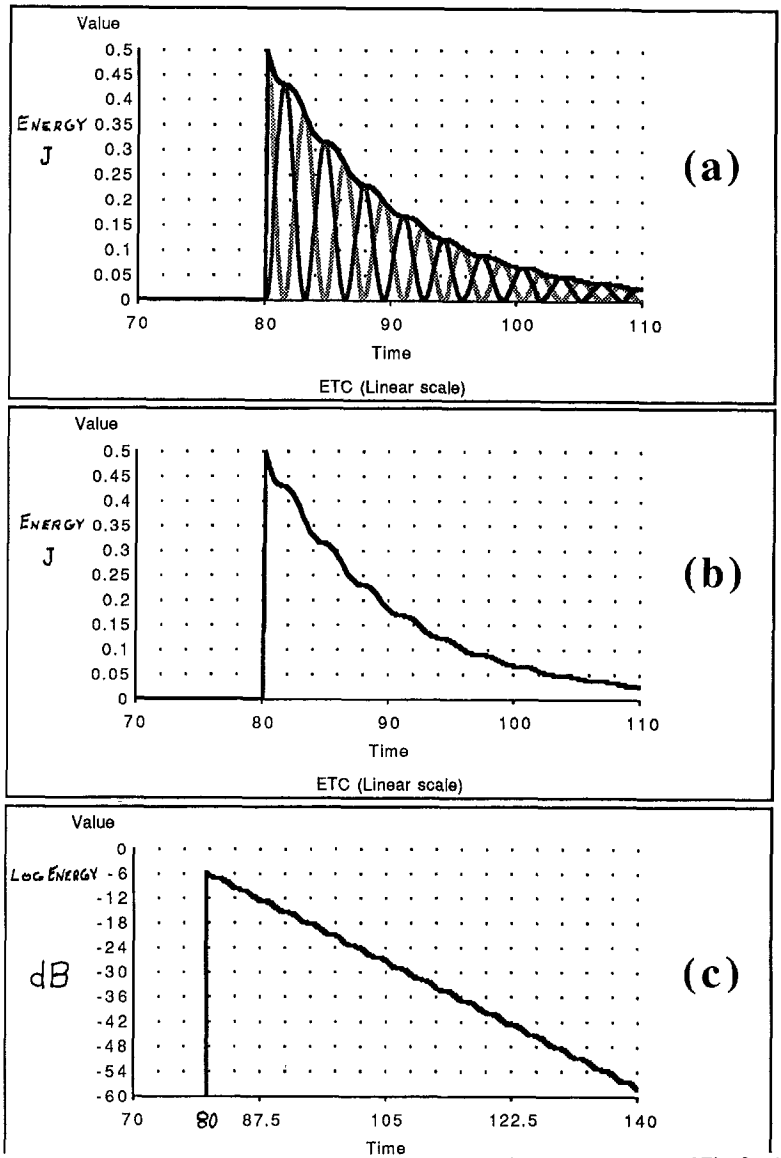

Fig. 11. Plots of the true energy decay versus time for the mass-spring-damper system of Fig. 9 calculated from the sum of the predicted potential and kinetic energies. The impulse of force is applied at t = 80 secs. (a) Energy decay plotted on a linear vertical scale (dark line) from 70 to 110 secs, with the instantaneous potential and kinetic energies shown in lighter lines. (b) Energy decay plotted on a linear vertical scale from 70 to 110 secs. (c) Energy decay plotted on a 60-dB log scale over the wider time range of 70 to 140 secs. Note that the energy does not decay in a purely exponential manner, but in a sequence of small steps synchronized with the oscillation. This is because the energy is dissipated only when the mass is in motion. Note the instantaneous jump in energy at 80 secs when the force impulse is applied.

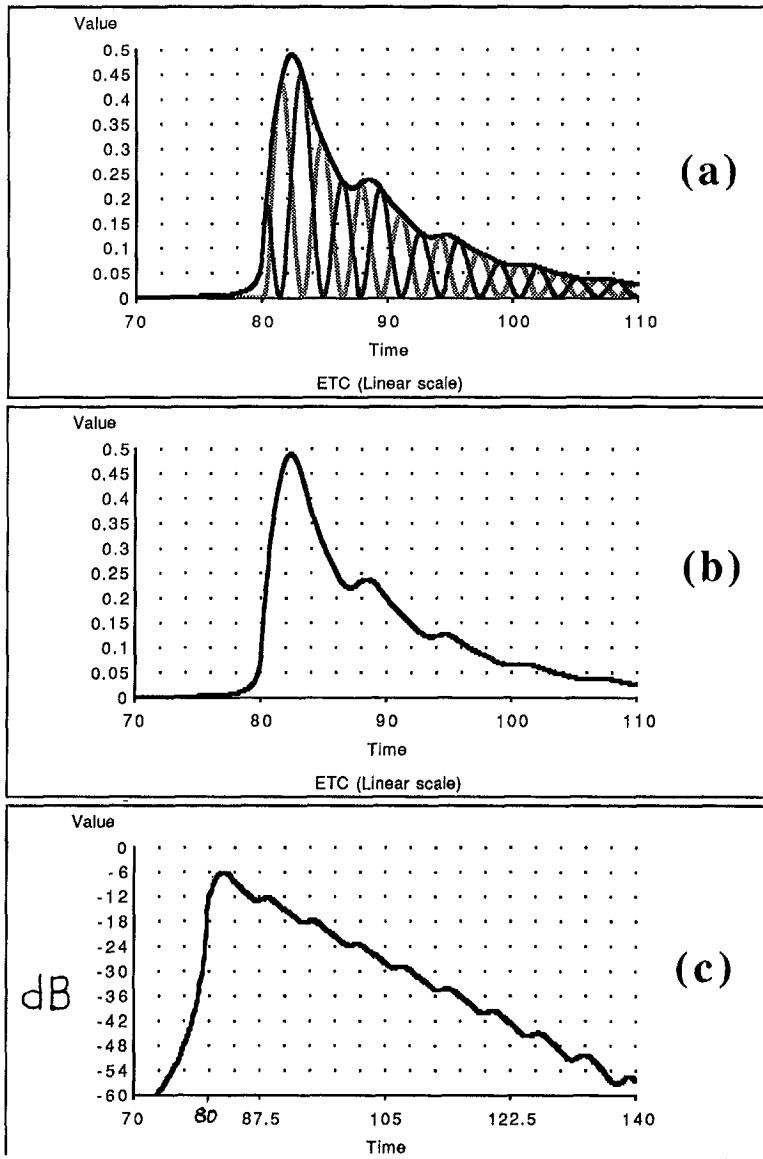

Fig. 12. Plots of the ETC predicted energy decay of the the mass-spring-damper system of Fig. 9 when the analytic impulse is applied at t = 80 secs. (a) ETC plotted on a linear vertical scale (dark line) from 70 to 110 secs, with the instantaneous squares of the real and imaginary parts of the analytic impulse response shown in lighter lines. (b) ETC plotted on a linear vertical scale (dark line) from 70 to 110 secs. (c) Energy decay plotted on a 60-dB log scale over the wider time range of 70 to 140 secs. Compare the plots in this figure with the true energy decay in Fig. 11. Note the rounding of the initial peak and the acausal build up of energy before the impulse that is a characteristic of the ETC. Note also that the small variations in the decay do not agree with the true energy decay of Fig. 11.